



**HAL**  
open science

## Controls on Dense Shelf Water formation in four East Antarctic polynyas

Esther Portela Rodriguez, Stephen Rintoul, Laura Herraiz-Borreguero, Fabien Roquet, Sophie Bestley, Esmee van Wijk, Takeshi Tamura, Clive McMahon, Christophe Guinet, Robert Harcourt, et al.

► **To cite this version:**

Esther Portela Rodriguez, Stephen Rintoul, Laura Herraiz-Borreguero, Fabien Roquet, Sophie Bestley, et al.. Controls on Dense Shelf Water formation in four East Antarctic polynyas. 2022. hal-03659459

**HAL Id: hal-03659459**

**<https://hal.science/hal-03659459>**

Preprint submitted on 5 May 2022

**HAL** is a multi-disciplinary open access archive for the deposit and dissemination of scientific research documents, whether they are published or not. The documents may come from teaching and research institutions in France or abroad, or from public or private research centers.

L'archive ouverte pluridisciplinaire **HAL**, est destinée au dépôt et à la diffusion de documents scientifiques de niveau recherche, publiés ou non, émanant des établissements d'enseignement et de recherche français ou étrangers, des laboratoires publics ou privés.

# Controls on Dense Shelf Water formation in four East Antarctic polynyas

Esther Portela<sup>1,2</sup>, Stephen R. Rintoul<sup>3,4,5</sup>, Laura Herraiz-Borreguero<sup>3,5</sup>, Fabien Roquet<sup>6</sup>, Sophie Bestley<sup>1,4</sup>, Esmee van Wijk<sup>3,4</sup>, Takeshi Tamura<sup>7,8</sup>, Clive R. McMahon<sup>1,9</sup>, Christophe Guinet<sup>10</sup>, Robert Harcourt<sup>11</sup>, and Mark A. Hindell<sup>1</sup>

<sup>1</sup>Institute for Marine and Antarctic Studies, University of Tasmania, Hobart 7001, Australia

<sup>2</sup>Univ. Brest, Laboratoire d'Océanographie Physique et Spatiale, CNRS, IRD, Ifremer, Plouzané, France

<sup>3</sup>Commonwealth Scientific and Industrial Research Organization (CSIRO) Oceans and Atmosphere, Hobart 7001, Australia

<sup>4</sup>Australian Antarctic Program Partnership, Institute for Marine and Antarctic Studies, University of Tasmania, Hobart 7001, Australia

<sup>5</sup>Centre for Southern Hemisphere Oceans Research Centre (CSHOR), Hobart 7001, Australia

<sup>6</sup>Department of Marine Sciences, University of Gothenburg, Gothenburg 40530, Sweden

<sup>7</sup>National Institute of Polar Research, Tachikawa 190-8518, Japan

<sup>8</sup>Graduate University for Advanced Studies (SOKENDAI), Tachikawa 190-8518, Japan

<sup>9</sup>Integrated Marine Observing System Animal Tagging sub-Facility, Sydney Institute of Marine Science, Mosman 2088, Australia

<sup>10</sup>Centre d'Etudes Biologiques de Chizé, CNRS, 79360 Villiers en Bois, France

<sup>11</sup>School of Natural Sciences, Macquarie University, Sydney 2109, Australia

## Key Points:

- Dense Shelf Water forms in Mackenzie Polynya but not in other nearby coastal polynyas.
- Relatively high salinity in early winter and high sea-ice formation favor Dense Shelf Water formation in Mackenzie Polynya.
- The properties and volume of DSW formed in a coastal polynya depend on its pre-conditioning as well as on sea-ice formation.

---

Corresponding author: Esther Portela, [eportelanh@gmail.com](mailto:eportelanh@gmail.com)

28 **Abstract**

29 Coastal polynyas are key formation regions for Dense Shelf Water (DSW) that ultimately contribute to the ventilation of the ocean abyss. However, not all polynyas form DSW. We examine how the physiographic setting, water-mass distribution and transformation, water column stratification, and sea-ice production regulate DSW formation in four East Antarctic coastal polynyas. We use a salt budget to estimate the relative contribution of sea-ice production, lateral advection, and vertical entrainment to the monthly change in salinity in each polynya. DSW forms in Mackenzie polynya due to a combination of physical features (shallow water depth and a broad continental shelf) and high sea-ice production. Sea-ice formation begins early (March) in Mackenzie polynya, counteracting fresh advection and establishing a salty mixed layer in autumn that preconditions the water column for deep convection in winter. Sea ice production is moderate in the other three polynyas, but saline DSW is not formed (a fresh variety is formed in the Barrier polynya). In the Shackleton polynya, brine rejection during winter is insufficient to overcome the very fresh autumn mixed layer. In Vincennes Bay, strong inflow of modified Circumpolar Deep Water stratifies the water column, hindering deep convection and DSW formation. Our study highlights that DSW formation in a given polynya depends on a complex combination of factors, some of which may be strongly altered under a changing climate, with potentially important consequences for the ventilation of the deep ocean, the global meridional overturning circulation, and the transport of ocean heat to Antarctic ice shelves.

48 **Plain Language Summary**

49 Coastal polynyas are regions of open water surrounded by sea ice. When annual sea ice forms, it is pushed off-shore by the strong winds blowing from the Antarctic continent. The salt that is released into the water below as the sea water continually re-freezes, increases salinity and density in the water column. In some polynyas, this water is dense enough to cascade down-slope from the continental shelf and supply a network of bottom ocean currents that influences global climate. In other polynyas the water in winter is not sufficiently dense to penetrate into the ocean abyss. Using data collected by instrumented elephant seals, we investigated the main factors controlling this dense water formation in four East Antarctic polynyas. We found that dense water production is dominated by the strength of sea-ice formation and by the salinity of the seawater at the beginning of the winter. The geographical and physical characteristics of the polynyas and regional circulation also modulate the final water density. Our findings provide insight into how dense water formation in East Antarctic polynyas might respond to future changes in climate influencing the transport of ocean heat to Antarctic continent and triggering the melt of the ice shelves.

64 **1 Introduction**

65 Coastal polynyas are regions of open water or low sea ice concentration where the ocean surface is directly exposed to the cold atmosphere. Persistent wind-driven sea ice export and winter heat loss in coastal polynyas results in continuous sea ice formation and brine rejection. In some polynyas, the buoyancy loss due to cooling and salinification is sufficient to drive deep convection and formation of Dense Shelf Water (DSW).

70 The cold and salty DSW that cascades down the Antarctic continental slope is the precursor of Antarctic Bottom Water (AABW), the densest water mass in the ocean. The down-slope transport of DSW and AABW formation play a crucial role in Earth's climate system, global deep-ocean circulation (Orsi et al., 1999; Jacobs, 2004), and biogeochemical cycles (Shapiro et al., 2003). They connect the surface waters, imprinted with the signal of exchange with the atmosphere, with the deep ocean and transport dense water and tracers

76 towards lower latitudes, ventilating the ocean abyss (Orsi et al., 2002; Foster & Carmack,  
77 1976).

78 The two major sites of AABW formation around Antarctica are the Weddell Sea and  
79 Ross Sea (Orsi et al., 2002). These regions host highly productive coastal polynyas on  
80 wide continental shelves with large neighboring ice shelves and cross-shelf depressions that  
81 have the capacity to accumulate and export large volumes of DSW (Gordon et al., 2004).  
82 In contrast, the Adélie Land source region is located on a narrower continental shelf with  
83 more limited storage capacity in East Antarctica, where the persistent Mertz polynya ac-  
84 tivity drives a relatively fresh Bottom Water supply (Gordon & Tchernia, 1972; Rintoul,  
85 1998; Williams et al., 2008). More recently, the Cape Darnley-Prydz Bay region has been  
86 identified as another region exporting DSW to form AABW (Ohshima et al., 2013; Herraiz-  
87 Borreguero et al., 2015, 2016; Williams et al., 2016; Portela et al., 2021). While these studies  
88 highlight the role of coastal polynyas in the formation of these dense-water overflows, DSW  
89 is noticeably absent in other coastal polynyas (Ribeiro et al., 2021; Silvano et al., 2018;  
90 Narayanan et al., 2019).

91 Previous studies have assessed the influence of cryospheric, oceanographic, and phys-  
92 iographic factors (Amblas & Dowdeswell, 2018; Baines & Condie, 1998; Narayanan et al.,  
93 2019) on DSW formation and export. While the primary mechanism for DSW formation  
94 is high sea-ice production and consequent salt rejection in coastal polynyas, physiographic  
95 factors (e.g. polynya size and depth, topography, and shelf geography), regional circula-  
96 tion, and the water masses present on the shelf likely modulate the production of DSW  
97 (Portela et al., 2021; Amblas & Dowdeswell, 2018; Narayanan et al., 2019; Liu et al., 2018).  
98 However, little is known about these interactions and their final effect on DSW formation.  
99 The absence of DSW in some polynyas has been attributed to the inflow of warm modified  
100 Circumpolar Deep Water (mCDW) onto the shelves leading to high basal melt rates of the  
101 adjoining glaciers (Ribeiro et al., 2021; Narayanan et al., 2019). The resulting freshwater  
102 outflow increases the stratification of the water column, hinders vertical convection and can  
103 thereby suppress the formation of DSW on the continental shelf (Silvano et al., 2018). The  
104 increased stratification, in turn, allows mCDW intrusions to reach the calving front of ice  
105 shelves. The presence of DSW in a given polynya can influence melt of nearby ice shelves  
106 in two ways. On the one hand, DSW has the potential to cause basal melt if it can access  
107 the grounding line, which is likely due to its high density. Due to the pressure dependence  
108 of the freezing point, the DSW is warmer than the in situ freezing point and therefore melts  
109 the underside of the ice shelf (Silvano et al., 2016; Jacobs et al., 1992). In addition, because  
110 DSW is denser than mCDW, the presence of DSW can also prevent warmer mCDW from  
111 reaching the grounding line (Jacobs et al., 1992), resulting in lower basal melt.

112 A better understanding of the factors regulating DSW formation in coastal polynyas  
113 will provide insight into the sensitivity of AABW formation and basal melt of ice shelves in  
114 a changing climate. The few decades of available DSW overflow records show a reduction of  
115 DSW export in some areas around Antarctica (Amblas & Dowdeswell, 2018). This apparent  
116 weakening of DSW formation on the Antarctic continental shelves may partly explain the  
117 observed changes in AABW (e.g. warming, freshening and volume reduction (Fox-Kemper  
118 et al., 2021; Purkey & Johnson, 2012; Kobayashi, 2018; Van Wijk & Rintoul, 2014)). This  
119 link between DSW formation and the change in AABW characteristics highlights the vari-  
120 ability of these complex ice-ocean systems and their vulnerability in the face of rapid climate  
121 change. Here, we use observations from four coastal polynyas to investigate the factors that  
122 favour or restrict formation of DSW. Our approach includes (i) investigation of water-mass  
123 transformation over winter, (ii) assessment of the role of preconditioning and (iii) compu-  
124 tation of a salt budget to estimate the relative contribution of brine rejection, entrainment  
125 and salt advection in driving observed monthly salinity changes. By comparing polynyas  
126 that do and do not produce DSW, we aim to gain improved understanding of the physical  
127 processes that regulate DSW formation, now and in the future.

## 2 Methods

We analysed four East Antarctic coastal polynyas: Mackenzie (MP), Barrier (BP), Shackleton (SP) and Vincennes Bay (VBP) (Figure 1). These polynyas were chosen because they have good temporal and spatial observational sampling by animal-borne sensors (section 2.1) during autumn-winter and their features cover a range of sea ice formation rates, geographic settings, and water mass distributions. As shown below, in the years they were best sampled, Mackenzie was an active source of DSW, Barrier was a weak source of relatively light DSW, and Shackleton and Vincennes Bay produced little or no DSW.

### 2.1 Data

The vertical temperature-salinity profiles used in this study were collected by southern elephant seals (*Mirounga leonina*) instrumented with Conductivity-Temperature-Depth Satellite-Relayed Data Loggers (CTD-SRDLs) during their annual post-moult (February - October) foraging trips. Southern elephant seals are excellent Southern Ocean samplers (Roquet et al., 2014; McMahon et al., 2021), and in particular have provided almost all the available data within Antarctic coastal polynyas during winter (Labrousse et al., 2018; Malpress et al., 2017). The profile data were retrieved from the Marine Mammals Exploring the Oceans Pole to Pole (MEOP) database (<http://www.meop.net/>), which is a comprehensive quality-controlled database (Roquet et al., 2014) that is an essential component of the global ocean observing system (GOOS). Additional data sources were explored, but sampling of coastal polynyas by more traditional oceanographic platforms (e.g. ships, floats and moorings) is comparatively sparse and not suitable.

For each coastal polynya, we analysed the year with the longest sampling record throughout the winter season. This means that data from different years are used in different polynyas: 2013 for MP, 2012 for BP and VBP, and 2011 for SP. The study area, as well as the location and date of the profiles collected by the tagged seals, is shown in Figure 1. Hereafter, all the analyses and comparisons refer to the selected year for each polynya.

To estimate the contribution of brine rejection to the salinity increase in each polynya, we used a daily sea-ice production dataset. Sea-ice production data was derived from special sensor microwave/imager (SSM/I) and special sensor microwave imager/sounder (SSMIS) data and atmospheric reanalysis from the ERA5 dataset. SIP data are seamlessly available for 28 years between 1992-2019. This dataset is similar to that of (Tamura et al., 2016), but uses different atmospheric forcing (ERA5 data are used in this study instead of ERA-interim).

### 2.2 Polynya identification

We identified polynyas using a combination of dynamic sea-ice concentration and static bathymetric data. The 12.5km resolution monthly SSM/I sea-ice concentration dataset (<ftp://ftp.ifremer.fr/ifremer/cersat/products/gridded/psi-concentration/data/>) was used to identify the polynya boundaries. In winter (from April to October) all data inside monthly sea-ice concentration contours of 75% were assigned to belong to the given polynya (Massom et al., 1998; Xu et al., 2017; Portela et al., 2021). With this method, polynya surface area changes monthly. In summer (from November to March), when most of the region is ice-free, we assigned profiles that were located within the 75% contours of mean sea-ice concentration between April and October of the preceding winter. To avoid including data off the continental shelf, the contours are further constrained by the continental slope (defined by depths > 1500 m). The bathymetry for the polynya regions was obtained from RTopo-2.0.4 Schaffer et al. (2019), (<https://doi.org/10.1594/PANGAEA.905295>).

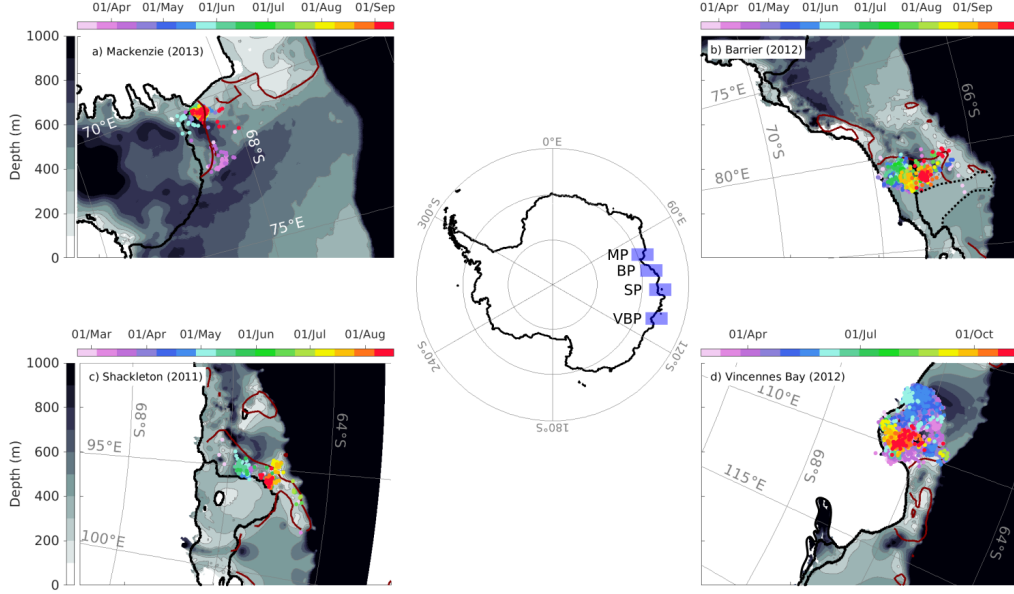


**Figure 1.** Location of vertical profile sampling (color-coded by time) within four East Antarctic coastal polynyas: a) 2013 Mackenzie (MP), b) 2012 Barrier (BP) c) 2011 Shackleton (SP) and d) 2012 Vincennes Bay (VBP).

### 2.3 Salt budget

The deepening of the mixed layer in coastal polynyas is driven by cooling and brine rejection during sea-ice production. As the mixed layer deepens, it entrains saltier water from below, further increasing the mixed layer salinity. In order to quantify the relative contribution of brine rejection, entrainment, and salt advection to the observed monthly salinity change ( $\Delta S_{Obs}$ ) in each polynya, we computed a salinity budget for the monthly-mean mixed layer and for the interior waters below. The method is illustrated in the schematic in Figure 2. Profiles within each month were used to compute the mixed layer depth using a density criterion of  $\Delta\sigma=0.03$  (de Boyer Montégut et al., 2004). The mixed layer depth and salinity were then averaged in each month. Changes in salinity in each layer were calculated as the difference between consecutive monthly means.

Within the mixed layer, monthly changes in the observed salinity,  $\Delta S_{Obs}$ , can be decomposed as:

$$\Delta S_{Obs} = \Delta S_{Brine} + \Delta S_{Ent} + \Delta S_{Adv} \quad (1)$$

Where  $\Delta S$  indicates the monthly salinity change centered on day 15 of each month, and the subscript indicates the contributing process:  $S_{Brine}$  for the salt released during sea ice formation (always positive),  $S_{Ent}$  for entrainment (always positive), and  $S_{Adv}$  for lateral salt advection (positive or negative).

$\Delta S_{Brine}$  was obtained by first computing the salt flux from the remotely-sensed sea-ice production estimates ( $Sf_{SIP}$ ) following Cavalieri and Martin (1994):

$$Sf_{SIP} = \rho_i V_i (S_{sw} - S_i) \cdot 10^3 \quad (2)$$

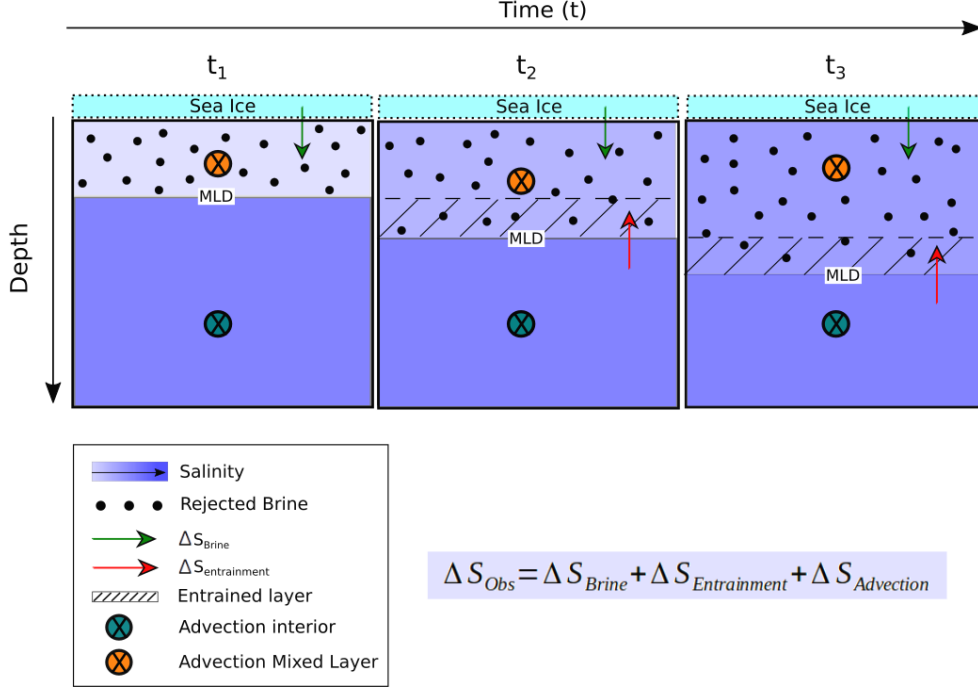


**Figure 2.** Schematic showing the processes considered in our salt budget computation as driving salinity change in the mixed layer and in the interior waters below. In this example, the process is schematised over three months ( $t_1 - t_3$ ).

193 Where  $\rho_i = 920 \text{ kg m}^{-3}$  is the sea ice density,  $V_i$  is the sea-ice production over the  
 194 polynya area in  $\text{m}^3$ ,  $S_{sw}$  is the mean seawater salinity in the region, and  $S_i$  is the frazil ice  
 195 salinity ( $S_i = 0.31 \times S_{sw}$ ). We then computed the salinity increase in a given month ( $t$ ) due  
 196 to this  $S_{SIP}^f$ :

$$\Delta S_{Brine_t} = \frac{S_{SIP}^f(t \rightarrow t+1)}{(\rho_{fw} V_{(ML)_{t+1}})} \quad (3)$$

197 Where  $\rho_{fw}$  is the freshwater density ( $1000 \text{ kg m}^{-3}$ ) and  $V_{(ML)}$  is the monthly mean  
 198 volume of the mixed layer.

199 The entrainment term was computed from the vertical temperature-salinity profiles.  
 200 The salt content ( $SC$ ) of the volume of water entrained into the mixed layer ( $V_{Ent} =$   
 201  $V_{(ML)_{t+1}} - V_{(ML)_t}$ ) during mixed layer deepening between two successive months ( $t$  and  
 202  $t + 1$ ), and its given salinity ( $S_{Ent}$ ), is:

$$SC_{Ent} = S_{Ent} \rho_{sw} V_{Ent(t \rightarrow t+1)} \quad (4)$$

203 The change in salinity of the mixed layer due to entrainment is then:

$$\Delta S_{Ent} = \frac{SC_{(ML)_t} + SC_{Ent(t \rightarrow t+1)}}{\rho_{fw} V_{(ML)_{t+1}}} - S_{(ML)_t} \quad (5)$$

Where  $\rho_{sw}$  is the monthly mean seawater density directly computed from the profile and  $\rho_{fw}$  is freshwater density. The  $\Delta S_{Ent}$  term was set to zero whenever the mixed layer depth remained unchanged or decreased in time.

Finally, the  $\Delta S_{Adv}$  was estimated as a residual, i.e.,  $(\Delta S_{Obs} - \Delta S_{Brine} - \Delta S_{Ent})$ . Below the mixed layer,  $\Delta S_{Obs}$  is only due to lateral salt advection. Observational errors, sparse seal sampling, and spatial variability could also contribute to the residual, but are not taken into account in our computation. Neglecting spatial variability within polynyas might be a strong assumption since, at least in the case of MP, water-mass distribution shows important spatial variability due to localised differences in bathymetry (Portela et al., 2021). However, for this study, most of the 2013 sampling in MP occurred over a limited area, thereby minimizing the effect of spatial variability. The importance of spatial variability is unknown for the other polynyas.

### 3 Results

The four polynyas analysed in this study show different physiographic characteristics. All four are located next to ice shelves but the ice shelf size, location within the bay, melt rate, and the influence of meltwater outflows from the ice shelf cavities differ. For instance, MP is situated next to the Amery ice shelf, the third largest in Antarctica, while VBP is adjacent to the smallest ice shelf considered in this study. MP and VBP both receive meltwater exported from the ice shelf cavities, which has been found to affect DSW formation there (Herraiz-Borreguero et al., 2015; Ribeiro et al., 2021). BP and SP are situated next to moderate-size ice shelves, the West and Shackleton ice shelves, respectively. These two ice shelves resemble ice tongues that may have multiple inflows and outflows from the ice shelf cavities, either within the polynyas or far away from them. Additionally, MP is located in western Prydz Bay, a region with a relatively wide continental shelf, while the other three polynyas are situated on narrow continental shelves and have their outer limits near the shelf break (Figure 1). Large ice shelves and wide continental shelves have been highlighted as factors favoring DSW formation by some authors (Narayanan et al., 2019), while others have recently pointed out that the presence of wide continental shelves are less important than previously thought (Amblas & Dowdeswell, 2018).

The four polynyas also differ in size (Figure 3a): SP is the largest ( $7.5 \pm 3.6 \times 10^3 \text{ km}^2$ ), followed by VBP and BP that have similar sizes ( $6.2 \pm 2.7 \times 10^3 \text{ km}^2$  and  $6.0 \pm 2.1 \times 10^3 \text{ km}^2$  respectively) and the smallest is MP (mean area  $3.9 \pm 2.1 \times 10^3 \text{ km}^2$ ). The values provided in parentheses are the mean areas reported by Nihashi and Ohshima (2015) for the period 2003-2011. In our study, mean polynya areas between May and October, computed as the integral of the grid cells with an ice concentration below 75%, are  $14.5 \times 10^3 \text{ km}^2$  in SP,  $12.4 \times 10^3 \text{ km}^2$  in BP,  $8.7 \times 10^3 \text{ km}^2$  in VBP and  $2.5 \times 10^3 \text{ km}^2$  in MP. Before March, polynya size cannot be estimated since the sea ice coverage is insufficient to define a polynya. By April, three of the four polynyas (MP, BP, and VBP) experienced a significant size reduction, they then remained approximately constant until August before re-opening in September (with the exception of MP, whose size did not increase again until December). SP exhibited different dynamics; its significant size reduction occurred a month later (by May) and it kept reducing in area until July, when its extent was at its minimum. It re-opened again in August and remained approximately constant until October. The sea ice concentration data, together with the changes in the area of each polynya, reveal MP in 2013 to be a small but active polynya, which forms early in the year (March) and persists for longer (until November) compared to the other polynyas, with relatively higher sea ice concentration. In contrast, SP was formed later and re-opened earlier than the other polynyas.

#### 3.1 Sea Ice production

The monthly mean of the spatially-averaged sea-ice production rate (Figure 4a) is independent of polynya size and provides a measure of the intensity of the brine rejected

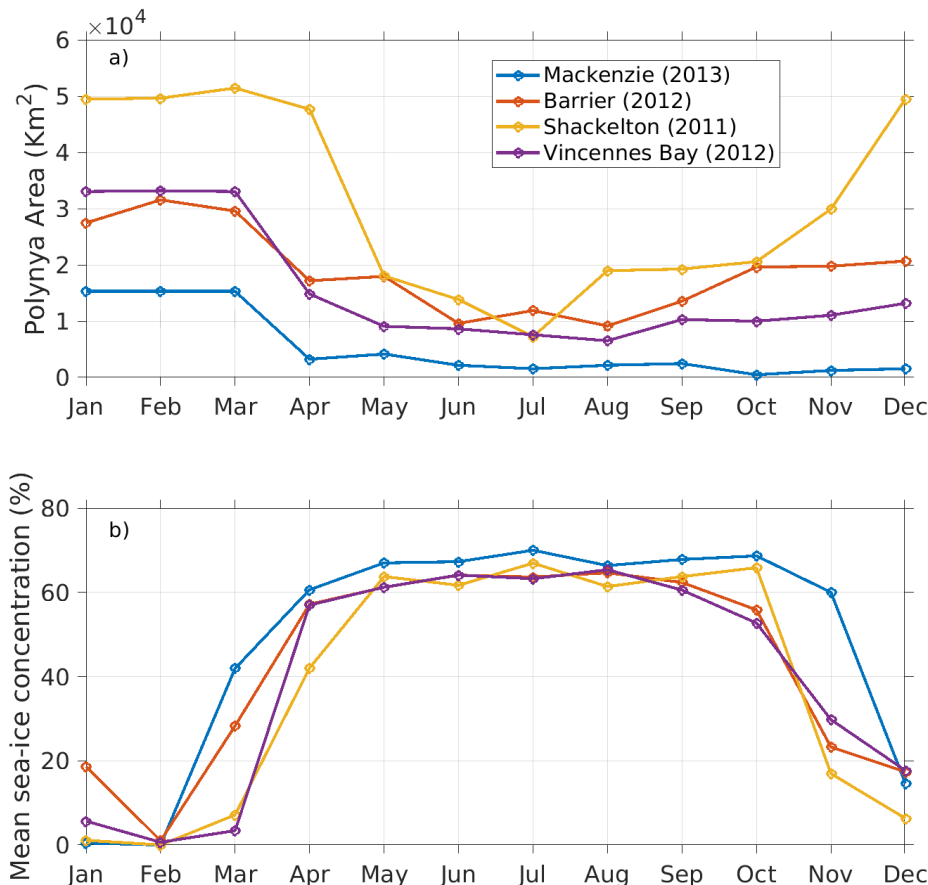


**Figure 3.** a) Area and b) sea ice concentration of the four polynyas investigated in this study. The sea ice concentration is the average within the polynya contour, defined by its sea ice concentration <75%, this means that this is the maximum possible value in panel b, only achieved if the sea ice concentration is 75% in every grid point within the polynya.

254 within each polynya. Therefore, this is the preferred parameter to assess the potential of  
 255 a given polynya to form DSW, as sea-ice production is directly related to salinity increase.  
 256 The sea-ice production rate is more than twice as strong in MP than in the other polynyas  
 257 between March and May, with its peak in April. From June onward sea-ice production  
 258 decreases, but it remains the highest of all four polynyas until September. Over the whole  
 259 winter (between March and October, inclusive), the accumulated sea-ice production in MP  
 260 is more than twice that of the other three polynyas: 13.4 m in MP, 5.5 m in BP, 6.5 m in  
 261 SP and 6.6 m in VBP.

### 262 3.2 Seasonal water-mass transformation

263 The water mass properties in each polynya between March and October (inclusive) are  
 264 shown in Figure 5 where the main water masses are labeled and the time is color-coded (see  
 265 Table 1 for water mass definitions). Note that while in SP and VBP there are data from  
 266 the beginning of March, in MP and BP the time series begins at the middle and the end of  
 267 March, respectively (see Figure 6).

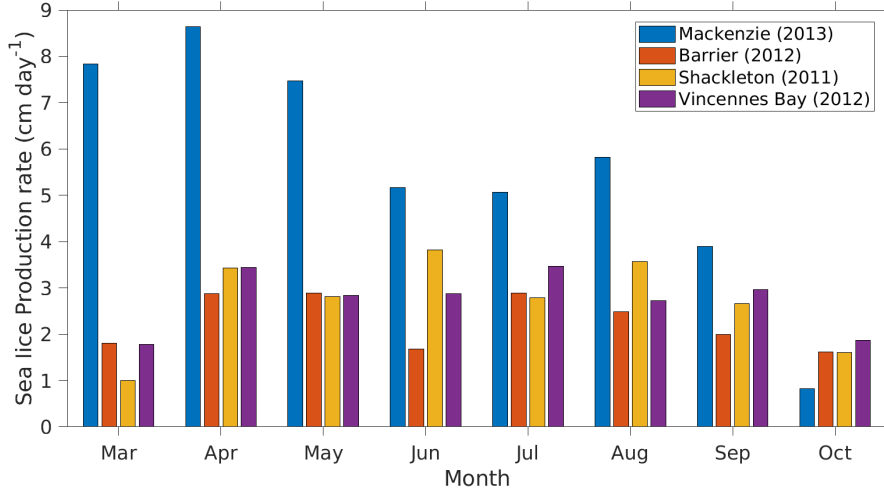


**Figure 4.** Monthly mean of the Sea Ice Production rate in each polynya between March and October.

268 The saltiest DSW is observed in MP, with a maximum salinity of about 34.7 reached  
 269 in mid September, the end of the sampling period here (Figures 5a and 6a). DSW is  
 270 also present in BP in September, with maximum salinity near 34.6 (Figures 5b and 6c).  
 271 In contrast, no DSW is observed in SP and VBP over the period of observations, which  
 272 extends until late August and November, respectively (Figures 5c, d and 6 e, g). In the  
 273 latter polynyas, salinity of waters near the surface freezing point (also named Low Salinity  
 274 Shelf Waters) reaches a maximum of  $\approx 34.45$  and  $\approx 34.5$ , respectively.

**Table 1.** Water-mass classification based on Herraiz-Borreguero et al. (2016, 2015); Williams et al. (2016) and Orsi and Wiederwohl (2009).

Water mass	Salinity	Potential temperature	Neutral density
AASW	$S < 34.4$	$\theta > T_f$	$\gamma < 28$
mCDW	-	$\theta > T_f + 0.1$	$28 < \gamma < 28.27$
ISW	-	$\theta < T_f - 0.05$	-
DSW	$S > 34.5$	$T_f - 0.05 < \theta < T_f + 0.1$	$\gamma > 28.27$

\* $T_f$ : surface freezing point.

275 Besides the presence or absence of DSW, all four polynyas differ greatly in terms of  
 276 water-mass distribution. mCDW is only present in MP in autumn, with a relatively cool  
 277 maximum temperature of  $-1.5$  °C. mCDW was only observed when the seal sampled the  
 278 eastern side of MP (Figure 1a), so it may reflect spatial variability of the water masses within  
 279 the polynya (Portela et al., 2021) and Prydz Bay (Herraiz-Borreguero et al., 2015). In BP,  
 280 mCDW is practically absent and only sporadically observed in SP. In contrast, mCDW is  
 281 widespread and particularly warm (maximum temperatures  $> 0.5$ °C) in VBP, in agreement  
 282 with previous observations encompassing wider or different periods (Ribeiro et al., 2021;  
 283 Kitade et al., 2014). Ice Shelf Water (ISW, Table 1) is present in MP and BP, the two  
 284 DSW-forming polynyas, but is relatively salty/dense in MP (density ranging between 27.5  
 285 and  $27.7$  kg m<sup>-3</sup>) compared to the fresher/lighter ISW in BP (density between 27.4 and

286 27.6 kg m<sup>-3</sup>) (Figures 5a, b). ISW is absent in SP and a relatively warm and fresh variety  
 287 is observed in VBP.

288 The properties of the AASW, the freshest water mass of the water column, also vary  
 289 between polynyas. April AASW is warmer and saltier in MP and VBP where its minimum  
 290 salinity ranges between 33.8 and 34 (Figures 5a, d and 6 a, g). In MP, warm AASW was only  
 291 sampled in the eastern part of the polynya (Figure 1a), with different water-mass properties  
 292 from the western part (Portela et al., 2021) . In contrast, AASW is colder and fresher in BP  
 293 and SP in April (minimum salinity of 33.4-33.5) (Figures 5b, c and 6 c, e). Fresh AASW  
 294 is also observed in VBP in March (S<33.6). However it rapidly becomes saltier in April  
 295 (S>33.8). The fresh surface layer in autumn reflects summer ice melt, and it cools and  
 296 salinifies as the winter progresses. Thus, the properties of the AASW in autumn (March-  
 297 April) depend on the oceanic heat loss and brine rejection in each polynya and on the  
 298 amount of melt that occurred over the previous summer. Saltier (therefore denser) AASW  
 299 in autumn is indicative of an earlier or more intense sea-ice production and/or less ice melt.  
 300 This results in the preconditioning of the water column that would reduce stratification and  
 301 favor further convection.

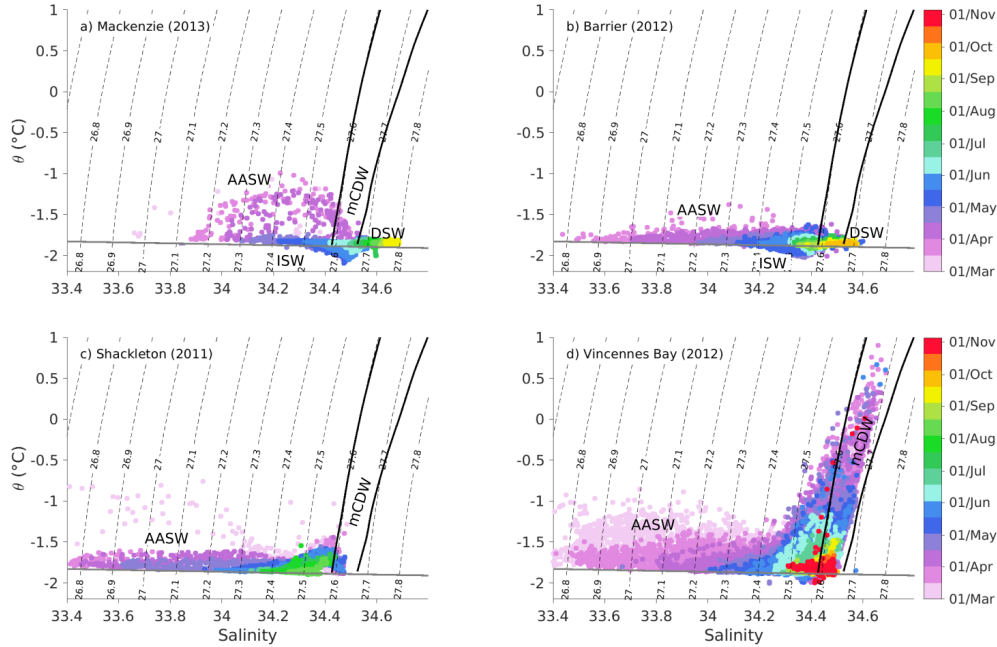


**Figure 5.** Potential temperature -salinity diagram in the four polynyas: (a) Mackenzie, (b) Barrier, (c) Shackleton, and (d) Vincennes Bay. The dashed lines are the isopycnals and the thick black contours highlight the isoneutrals of 28 and 28.27 kg m<sup>3</sup> that delimit the mCDW

302 The vertical distribution of the water masses with time provides additional information  
 303 on how they are transformed over the winter (Figure 6 left column, a, c, e, g). In Figure 6  
 304 each water mass is represented with a different color palette. To avoid over-plotting, we have  
 305 used the daily average of all data available within each polynya in their particular year. This  
 306 representation highlights the role of the different water masses in setting the stratification  
 307 ( $N^2$ ) of the water column (Figure 6b, d, f, h) and thus, influencing the formation and  
 308 evolution of DSW.

309 In MP, remnant DSW below the mixed layer (S=34.5, blue dots in Figure 6a) is observed  
 310 throughout the entire sampling period except between mid April and mid May, when ISW

(pink) is observed in the bottom layer instead. This ISW is as salty as the remnant DSW so it is similarly dense. Full convection is achieved and new DSW is formed in MP episodically from early June, and more consistently from July. This DSW gets progressively saltier until mid-September, the end of the sampling record (Figures 5a and 6 a).

In BP only episodic remnant DSW is found in late summer, but most of the seafloor is occupied by relatively fresh ( $S=34.4$ ) ISW in April and early May. Similarly fresh mCDW is observed during the same period. Full convection is achieved in late June, but new DSW is not consistently formed until August, reaching maximum salinity about 34.55 by the end of September (Figures 5b and 6c). In both MP, and BP, the shallow bathymetry in comparison with the two other polynyas might have also contributed to achieve full convection earlier in the year.

In SP the water column is fully occupied by AASW, except for the bottom layer ( $> 500\text{m}$  depth) which is occupied by mCDW. Despite a relatively weak stratification compared with the other polynyas (Figure 6f), full convection is never achieved and salinity by mid-August (end of the time series) remains too low to form DSW (Figures 5c and 6e). Due to data limitations, we cannot know if there was DSW formation later in the year, and the seals did not sample SP in winter in any other year.

In the relatively deep VBP embayment, the water-column structure consists of AASW overlying a thick layer of warm mCDW during the entire March to November period (with a data gap in July-August). The mixed layer deepens progressively from early April until the end of June, when it reaches more than 500 m. However, by this time, full convection is not yet achieved, and mCDW still underlies the AASW above. By September, after the winter data gap, the mixed layer is very variable, but it does not reach the bottom of the dive profile. Despite the lack of detailed observations spanning the entire winter period, there is evidence that the mixed layer starts shallowing again by the beginning of October.

The stratification of the water column, as represented by  $N^2$ , is a measure of the stability of the water column. Weaker stratification favors full convection and DSW formation. Stratification is of similar magnitude and follows similar temporal variability in MP and BP (with maximum slightly stronger in BP, Figure S1), it is slightly weaker in SP, and much stronger in VBP (Figure 6 b, d, f, h). However, this must be interpreted in combination with the water-mass properties in order to gain insight into the processes governing DSW formation. The weaker stratification in SP (Figure 6f, S1) reflects the dominance of AASW within the water column, resulting in water properties that change more smoothly over depth. However, mixed layer salinity is very low and, even if the stratification is weak, the buoyancy flux is not strong enough to induce convection. In BP, SP and VBP, the maximum stratification between March and May (Figure S1) corresponds with the abrupt vertical salinity changes associated with very fresh AASW ( $S<33.6$ ) occupying the mixed layer. In MP, this fresh AASW is absent, and the stratification is mainly set by the contrast between relatively salty AASW within the mixed layer, and the saltier DSW or ISW below (Figure 6).

### 3.3 The role of preconditioning

Low initial salinity needs stronger transformation to achieve the threshold DSW salinity of 34.5. Therefore, mixed layer salinity at the beginning of the winter is potentially an important factor influencing DSW formation. The difference between the salinity within the mixed layer and right below (another indirect measure of stratification) (Figure 7), determines the buoyancy flux needed for achieving convection. For example, at similar sea-ice production rate, mixing with saltier waters below as the winter draws on will increase the mixed layer salinity faster.

In MP, two features favorable to DSW formation occur by early April: (i) the mixed layer waters are already relatively salty ( $S\approx 34$  compared with  $\approx 33.7$  in BP, 33.85 in VBP

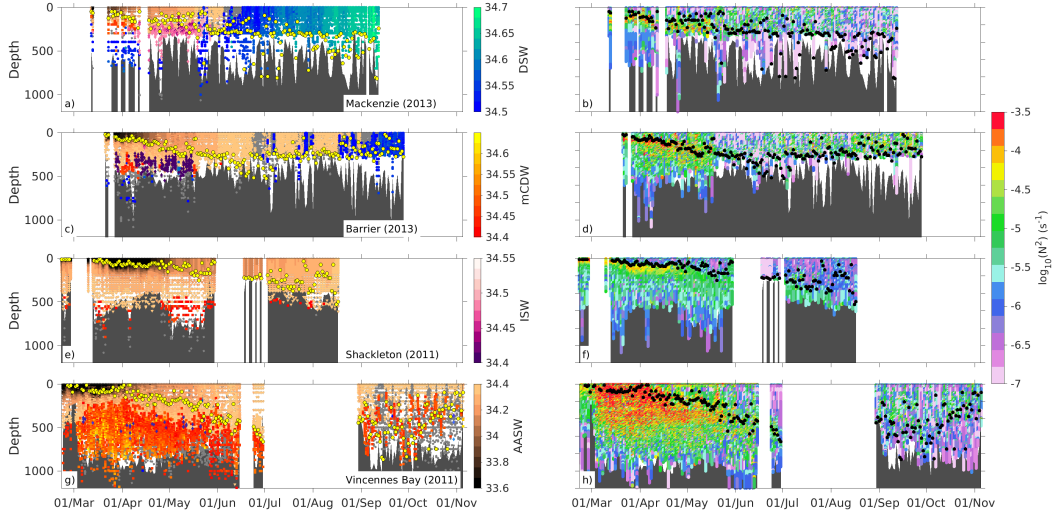


**Figure 6.** Time line of water column salinity (left column), highlighting the different water masses and their seasonal transformation across the four polynyas, and their stratification given by  $N^2$  (right column). (a-b) Mackenzie, (c-d) Barrier, (e-f) Shackleton, and (g-h) Vincennes Bay. For clarity, each water mass is shown with a different color palette. Grey dots represent the transitional water masses before the minimum DSW salinity is reached at a temperature near the freezing point (sometimes defined as Low Salinity Shelf Water (LSSW) (Gordon & Tchernia, 1972)). The bathymetry is shaded in grey and the yellow dots (black in right column) represent the mixed layer depth as computed with a  $\Delta\sigma$  criterion of  $0.03 \text{ kg m}^{-3}$  (de Boyer Montégut et al., 2004)

361 and 33.5 in SP), (ii) interior waters are saltier than in the other polynyas ( $S \approx 34.4$  in MP,  
 362 compared with  $S \approx 34.15$  in BP and VBP, and  $S \approx 33.8$  in SP). As a result, (iii) in MP,  
 363 the salinity of both layers converge quickly, reaching the threshold DSW salinity (34.5) by  
 364 the beginning of June and increasing smoothly until September. In contrast salinity stays  
 365 constant in BP over the same period (June-September). Unfortunately, the sampling gap  
 366 in VBP hinders the assessment of its seasonal transformation.

367 Despite the initial salinity differences between the mixed layer and below, BP, SP, and  
 368 VBP all exhibit a rapid salinification during the month of April. In MP, the salinity increase  
 369 occurs at slightly lower rate in the first half of April, and slows down from mid April. This  
 370 contrasts with the sea-ice production rate observed in MP (Figure 4a) that was double that  
 371 of the other polynyas. The lower rate of salinity increase in MP in April might be related to  
 372 the spatial variability of the sampling, as the seal traveled from the eastern to the western  
 373 side of the polynya during this month. Our previous study highlighted important differences  
 374 in water-mass properties between the eastern and western areas within MP (Portela et al.,  
 375 2021). By May, the differences between polynyas has reduced. The salinity of both layers  
 376 is similar in MP, BP and VBP to the beginning of July, when full convection is achieved  
 377 in both MP and BP (Figure 6a-d) and the rate of salinity increase slows down in all four  
 378 polynyas.

### 379 3.4 Salinity balance

380 To better understand the processes driving the observed monthly changes in salinity  
 381 ( $\Delta S_{obs}$ ), and therefore the potential for DSW formation in each polynya, we calculated three  
 382 terms contributing to the salt balance: brine rejection due to sea-ice production, entrainment

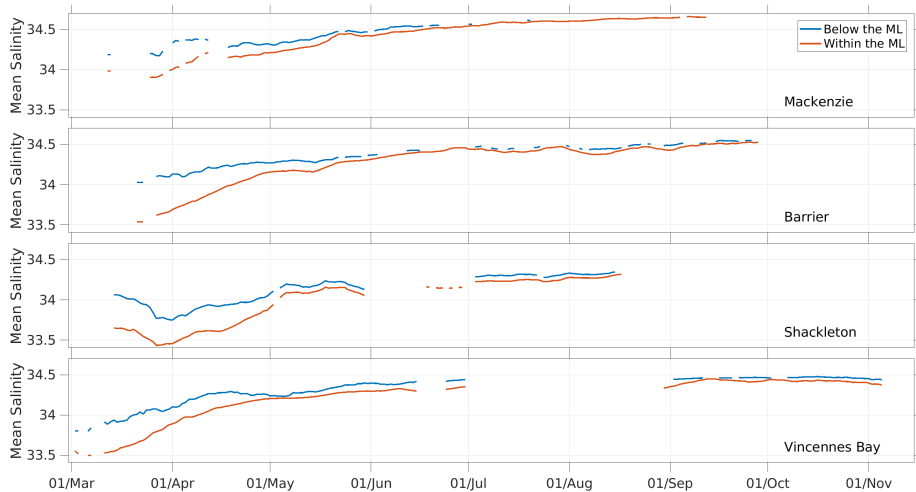


**Figure 7.** Temporal evolution of mean salinity within the mixed layer (red line), and within the 100 m below the mixed layer (blue line) or to the seafloor where shallower. (a) Mackenzie, (b) Barrier, (c) Shackleton, and (d) Vincennes Bay.

383 during mixed layer deepening, and lateral advection (as a residual), using equations 1 to 5  
 384 (see Methods).

385 In MP (Figure 8a), brine rejection from sea-ice production dominates the observed  
 386 salinity increase, which is partially offset by advection of relatively fresh waters within  
 387 the mixed layer. The inferred advection of fresh water during most of the winter might  
 388 reflect meltwater inflow as reported previously (Herraiz-Borreguero et al., 2015, 2016), or  
 389 the transport of fresh AASW into the polynya. Advection in the mixed layer appears  
 390 decoupled from that in the interior (where advection of salty water occurs). This contrasts  
 391 with the other three polynyas where salt advection follows a similar pattern throughout the  
 392 water column.

393 Below the mixed layer, the strong positive salt advection suggests inflow of salty water  
 394 masses such as DSW or mCDW directly into MP. Since the presence of mCDW has not been  
 395 detected (Figure 6a), we hypothesize that MP might be receiving DSW in the interior layer  
 396 from other upstream Prydz Bay polynyas (such as BP) (Herraiz-Borreguero et al., 2016;  
 397 Williams et al., 2016) or possibly the neighbouring Darnley polynya (Portela et al., 2021).  
 398 Spatial variability within MP could also explain our results since bathymetry strongly influ-  
 399 ences the water-mass distribution below the mixed layer (Portela et al., 2021). Entrainment  
 400 accounts for about a third of the  $\Delta S_{obs}$  in April, less than a fifth in May, and is reduced  
 401 to zero thereafter when the mixed layer depth approaches the seafloor (Figure 8). This is a  
 402 common feature across the four polynyas: entrainment makes a larger contribution to the  
 403 salinity increase in the mixed layer in early winter, when the salinity contrast between the  
 404 mixed layer and the interior is large. As the mixed-layer salinity increases during winter  
 405 and approaches that of the interior, the salinity increase from entrainment decreases. Addi-  
 406 tionally, as the mixed layer deepens, the salt added during entrainment results in a smaller  
 407 salinity increase overall.

408 In BP the salinity increase in the mixed layer from April to June is driven by a combi-  
 409 nation of brine rejection, salt advection and, to a lesser extent, entrainment. From June to  
 410 September, brine rejection acts to increase salinity, but is almost completely offset by fresh  
 411 advection between July and August. Based on the salinity profiles in Figure 6c, the inferred

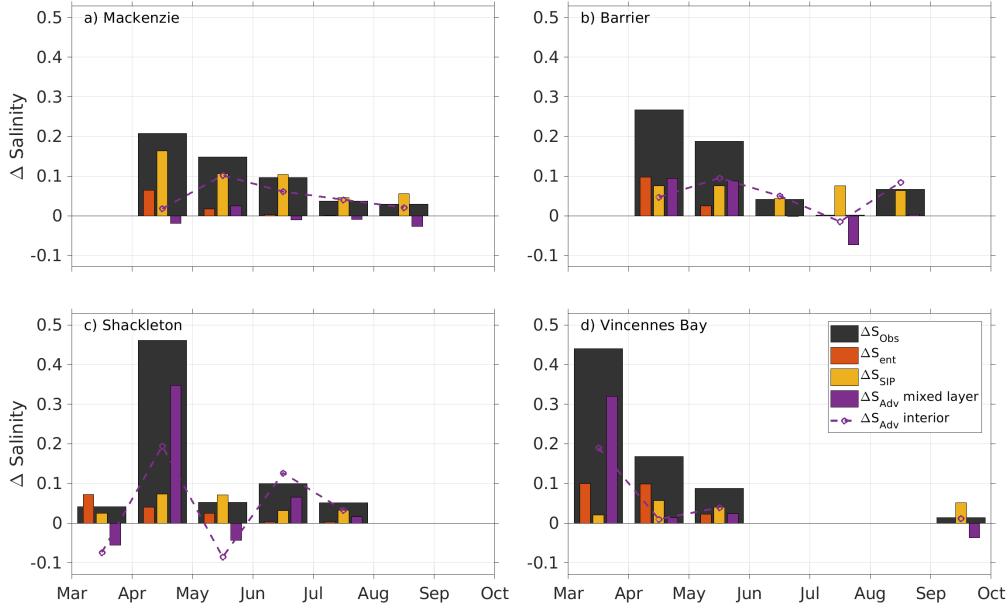


**Figure 8.** Monthly observed salinity increase and the relative contribution of brine rejection due to sea-ice production, entrainment, and advection for (a) Mackenzie (MP), (b) Barrier (BP), (c) Shackleton (SP), and (d) Vincennes Bay (VBP). The salt budget is computed within the dynamic mixed layer (bars); below the mixed layer (dashed line) the only contribution is advection.

412 advection might reflect inflow of relatively fresh AASW into the mixed layer once DSW has  
 413 started to form.

414 In SP and VBP, strong salinity increase due to inferred advection of salty waters is  
 415 observed in autumn (Figure 8c, d). This might be caused by the inflow of mCDW or a salty  
 416 AASW. In VBP, mCDW is widespread, whereas AASW is the dominant water mass in SP,  
 417 and mCDW is rarely observed there (Figure 6e, g). Rapid mixing between AASW and  
 418 mCDW could explain the rapid increase in mixed layer salinity observed in both polynyas  
 419 prior to May that is not explained by brine rejection. This scenario is also consistent with  
 420 the temperature increase observed in the interior AASW from April to May (Figure S2,  
 421 Supplementary Information). From May onward, the salinity increase in SP and VBP is  
 422 moderate ( $< 0.1$ ), and mainly attributed to brine rejection and salt advection in SP, and to  
 423 a combination of all terms in VBP. In the latter, the sea-ice production is still important in  
 424 September, after the sampling gap, but the salinity increase due to brine rejection is largely  
 425 offset by fresh advection.

426 The total salinity increase within the mixed layer between April and August (the com-  
 427 mon period across at least three polynyas) was 0.49 in MP, 0.50 in BP and, 0.67 in SP  
 428 (Figure 8). Due to the observational data gap this cannot be assessed in the same way for  
 429 VBP. The fact that the total salinity increase between April and August is the smallest in  
 430 MP, which forms DSW, and largest in SP, which does not, is revealing. This suggests that  
 431 a combination of factors determines whether or not DSW is formed in a given polynya, as  
 432 discussed below.

## 4 Discussion

Here we investigated several factors influencing DSW formation in four East Antarctic polynyas with different characteristics. We analysed the sea-ice production rate, water-mass distribution and seasonal transformation, and mixed layer depth. Using a salt budget, we estimated the relative contribution of brine rejection, entrainment, and salt advection to the monthly salinity change in and below the mixed layer in each polynya. Table 2 summarises the characteristics of each polynya and the factors influencing DSW formation. In MP, which had the strongest DSW formation, most factors are favourable. At BP, which exhibits weak formation of lighter DSW, most factors are favourable or neutral. Conversely, most factors hinder DSW formation in SP and VBP, where DSW is not observed.

**Table 2.** Summary of the main physiographic and hydrographic characteristics of each polynya and the factors evaluated in this study. The green and red shading highlight conditions that favour and hinder DSW formation respectively, while yellow shading indicates neutral conditions.

	Mackenzie	Barrier	Shackleton	Vincennes Bay
Year	2013	2012	2011	2012
Period	Mar-Sep	Mar Sep	Feb-Aug	Feb-Nov
Area	3000 km <sup>2</sup>	15000 km <sup>2</sup>	28000 km <sup>2</sup>	14000 km <sup>2</sup>
Bathymetry	300-600	300-600	600	> 1000
DSW formation	Yes	Little	No	No
Ice shelf	Yes	Yes	Yes	Yes, small
Continental shelf	Wide	Narrow	Narrow	Narrow
DSW Remnant	Yes	Minor	No	No
Initial Salinity (Interior)	High (34.4)	Medium (34.15)	Low (33.8)	Medium (34.15)
Initial Salinity (ML)	High (34)	Medium (33.7)	Low (33.5)	Medium (33.85)
ISW	Yes, salty	Yes, fresh	No	No
mCDW	Little, early	Little, cold	Little, fresh	Strong, warm, salty
AASW	Little, cold, salty	Yes	Yes, fresh	Yes, fresh
Full convection	July	June	Never	Uncertain (August)
Stratification	Medium	Medium	Weak	Strong
Mean SIP rate (cm day <sup>-1</sup> )	High (5.6)	Medium (2.3)	Medium (2.7)	Medium (2.7)

The particularly high sea-ice production rate in MP clearly favoured DSW formation there. The accumulated sea-ice production over the whole winter was twice as large in MP as in the other three polynyas (Figure 4). The difference was particularly large between March and May, when sea-ice production was strongest in MP. However, we found that DSW formation was not linked to sea-ice production alone. While sea-ice production remained high throughout the winter in MP, the increase in the mixed-layer salinity between April and August was the lowest of all polynyas (Figure 8a). The mixed layer salt budget suggests that the strong sea-ice production was partially offset by fresh advection during this period. The fresh advection likely reflects glacial meltwater entering MP from the cavity beneath the Amery Ice Shelf, which undergoes a net basal melt rate of  $57.4 \pm 25.3$  Gt yr<sup>-1</sup> ( $1 \pm 0.4$  m yr<sup>-1</sup>) (Herraiz-Borreguero et al., 2016). Another possibility is that MP received inflow of fresh AASW from neighboring areas with more sea-ice melt. However, this seems less likely given that the direction of sea ice drift was offshore (Figure S3).

Formation of DSW in MP was favored by the relatively high salinity observed throughout the water column from the beginning of the sampling record in March. The high salinity at the end of autumn means that less salt needs to be added to reach the salinity threshold

459 for DSW formation. The high salinity in March could reflect (i) preconditioning of the  
 460 interior waters by the presence or advection of DSW formed during the previous winter,  
 461 (ii) sea ice formation commencing earlier than in the other polynyas, and (iii) less sea-ice  
 462 melt in MP over summer. Option (i) would be consistent with the inferred advection of  
 463 salty water below the mixed layer. However, this is surprising given evidence that glacial  
 464 meltwater from the Amery Ice Shelf reaches MP (Herraiz-Borreguero et al., 2016). One  
 465 possibility is that MP does indeed receive meltwater input below the mixed layer, but that  
 466 this contribution is overwhelmed by lateral advection of salty waters into the region.

467 The presence of salty water below the mixed layer (either remnant DSW or from lateral  
 468 advection) might contribute to a saltier mixed layer through vertical entrainment. However,  
 469 the salt budget suggests that the contribution of entrainment to the observed salinity in-  
 470 crease was small in MP. Thus, even if the interior water salinity is high, it is not likely to  
 471 explain the high salinity observed in Autumn in MP.

472 The observation that the mixed layer (i.e. AASW) salinity in MP was higher at the  
 473 end of March than in the other polynyas provides support for option (ii) (sea-ice formation  
 474 commencing earlier than in the other polynyas). The salinity increase in autumn in MP was  
 475 also consistent with the estimated brine rejection (Figure 7). While warm surface waters  
 476 in late summer can bias estimates of sea-ice production (Tamura et al., 2007), the March  
 477 surface temperature approaches the freezing point in all four polynyas (Figure S2), providing  
 478 good confidence in the sea-ice formation estimates used here. In addition, the rapid increase  
 479 in sea-ice concentration in MP from 0% in February to 40% in March (Figure 3) in MP,  
 480 compared with 30% in BP, and <10% in SP and VBP for the same period, provides further  
 481 evidence of early and strong sea ice formation in MP.

482 High mixed layer salinity in MP at the start of winter might also be related to less sea-  
 483 ice melt over summer due to enhanced sea-ice export (option (iii)). This is consistent with  
 484 the strong and persistent katabatic winds blowing sea ice offshore in this region (Massom  
 485 et al., 1998). To test this idea, we computed monthly sea-ice divergence in each polynya  
 486 (Figure S3). The sea-ice velocity vectors suggest that sea-ice was constantly exported from  
 487 MP to the north, where there is sea-ice convergence. However, the results are inconclusive  
 488 due to insufficient spatial resolution of the sea ice drift dataset to resolve polynyas.

489 In contrast to MP, in the other polynyas the changes in monthly-mean salinity did  
 490 not track sea-ice production. The other terms in the salt balance (entrainment and lateral  
 491 advection) are often as large or larger than sea ice formation (Figure 8). In BP, the salinity  
 492 of the mixed layer increased more rapidly from March to May than in MP, despite weaker sea  
 493 ice formation, due to salt input by entrainment and lateral advection. However, the initial  
 494 salinity was much lower than in MP, therefore, the salinity increase through the winter was  
 495 only sufficient to form a light variety of DSW. While BP and MP exhibited a number of  
 496 similar characteristics (e.g. shallow bathymetry, early full convection, absence of MCDW,  
 497 and similar stratification), the weaker sea ice formation and fresh conditions at the start of  
 498 winter conspire to limit DSW formation in BP. The fresher and lighter ISW observed at BP  
 499 might also increase stratification, inhibiting deep convection there. For instance, maximum  
 500 stratification in BP corresponds with the period where ISW observed (Figure S1).

501 While sea-ice production rates in SP and VBP were similar to that in BP, DSW was not  
 502 formed in SP and VBP. In SP, DSW formation was hindered by the presence of a thick layer  
 503 of very fresh AASW from late March. One explanation for this particularly fresh AASW  
 504 could be inflow of meltwater from either the Shackleton Ice Shelf or from the Denman glacier  
 505 flowing west under the Shackleton ice shelf, but we cannot corroborate this with the data in  
 506 hand. The overall winter increase in mixed layer salinity was much larger at SP than at MP  
 507 or BP (the data gap means this can't be assessed for VBP), despite sea ice production lower  
 508 than MP or similar to BP, largely as a result of very strong salt advection from April to May.  
 509 However, the combined salt input by brine rejection and advection was still insufficient to  
 510 overcome the initial low salinity of the AASW, drive full convection, and form DSW.

511 VBP, like SP, showed a strong increase in mixed layer salinity at the start of the winter  
 512 as a result of lateral advection (Figure 8). The mixed layer salinity at the start of the winter  
 513 was not as low as at SP, but was lower than at MP. The VBP polynya therefore did not  
 514 have to overcome as large a mixed layer salinity deficit as at SP. However, the presence of  
 515 mCDW below the surface mixed layer produced strong stratification (Kitade et al., 2014;  
 516 Ribeiro et al., 2021) that provided a barrier to full-depth convection and DSW formation.  
 517 At both SP and VBP, the absence of remnant DSW means that the waters below the mixed  
 518 layer was relatively fresh and the salinity of the entire water column must be increased by  
 519 a larger amount than at MP (and to a lesser extent, BP) to reach the threshold for DSW  
 520 formation.

521 In addition to the hydrographic properties and the sea-ice production rate, physio-  
 522 graphic features influenced the DSW formation in the four polynyas. MP is located on  
 523 a wide continental shelf, while the other three polynyas are located on narrower shelves.  
 524 Narrow continental shelves allow less time for DSW retention and salinification before the  
 525 dense water cascades offshore (Amblas & Dowdeswell, 2018). The physiographic features  
 526 of MP (shallow waters, wide continental shelf and presence of a large ice shelf) have been  
 527 previously identified as favorable for DSW production (Amblas & Dowdeswell, 2018), al-  
 528 though a wide shelf is not a requirement for DSW formation (Amblas & Dowdeswell, 2018;  
 529 Narayanan et al., 2019). The polynya size has influence on the total amount of DSW formed  
 530 in a given polynya if the density threshold is reached. However, it is unrelated to the sea-ice  
 531 production rate, therefore, polynya size is not a direct factor influencing on DSW formation.

532 Our analysis is limited to specific years, so presence or absence of DSW in our observa-  
 533 tions does not preclude DSW formation at a different time. Indeed, it has been shown that  
 534 polynyas exhibit interannual variability (e.g., Portela et al. (2021)), especially regarding the  
 535 structure of the water masses present. However, the absence of remnant DSW at SP and  
 536 VBP, and the fresh waters observed at depth there, suggest that DSW did not form in the  
 537 year prior to our observations in those polynyas. In any case, our focus here is on identifying  
 538 the physiographic, oceanographic and cryospheric factors that determine why DSW forms  
 539 in some coastal polynyas and not others. By focusing on specific polynyas in particular  
 540 years, we are able to explore in detail the factors that control DSW formation. This work  
 541 therefore complements recent circumpolar assessments spanning a longer time period that  
 542 investigate more general features (Amblas & Dowdeswell, 2018; Narayanan et al., 2019).

543 We show that DSW formation in Antarctic coastal polynyas is influenced by precon-  
 544 ditioning (e.g. salinity and stratification at the start of winter), lateral advection, and  
 545 physiographic factors, as well as sea ice formation rates. By demonstrating the sensitivity  
 546 of DSW formation to multiple factors, our study provides novel insights into how DSW for-  
 547 mation might respond to future changes in climate. Changes in wind strength and direction  
 548 that lead to changes in polynya size and sea ice production, are an obvious potential driver  
 549 of change in DSW formation. Changes in wind forcing may also drive changes in circula-  
 550 tion that alter the salinity and stratification of the water column (i.e. preconditioning) and  
 551 hence the susceptibility to full-depth convection. Increased glacial melt will likely enhance  
 552 stratification and limit DSW formation, with potential feedback on glacial melt (Silvano et  
 553 al., 2018). Climate variability and change may disrupt the delicate balance of factors that  
 554 control DSW formation. Previous observations and paleoceanographic evidence show that  
 555 DSW formation has varied on timescales from years to millennia (de Boer et al., 2007; Smith  
 556 et al., 2010)). Future changes in climate are likely to alter the factors influencing DSW for-  
 557 mation, and therefore bottom water formation and the deep overturning circulation, with  
 558 important consequences for climate, ventilation of the deep ocean, and ocean-driven melt  
 559 of Antarctic ice shelves.

## 560 Acronyms

561 **MP** Mackenzie polynya

562 **BP** Barrier polynya  
 563 **SP** Shackleton polynya  
 564 **VBP** Vincennes Bay polynya  
 565 **DSW** Dense shelf Water  
 566 **AASW** Antarctic Surface Water  
 567 **mCDW** modified Circumpolar Deep Water  
 568 **ISW** Ice Shelf Water  
 569 **AABW** Antarctic Bottom Water

## 570 **Acknowledgments**

571 The seal CTD-SRDL tags and deployment were funded and supported through a collabora-  
 572 tion between the French Polar Institute (program 109: PI. H. Weimerskirch and 1201: PI.  
 573 C. Gilbert and C. Guinet), the SNO-MEMO and CNES-TOSCA and the Integrated Marine  
 574 Observing System. Australia’s Integrated Marine Observing System (IMOS) is enabled by  
 575 the National Collaborative Research Infrastructure Strategy (NCRIS). It is operated by a  
 576 consortium of institutions as an unincorporated joint venture, with the University of Tasma-  
 577 nia as Lead Agent. [www.imos.org.au](http://www.imos.org.au). The Australian Research Council provided financial  
 578 support through Discovery Project DP180101667, under which E.P. is supported. S.B is  
 579 supported under ARC DECRA grant DE180100828. The marine mammal data were col-  
 580 lected and made freely available by the International MEOP Consortium and the national  
 581 programs that contribute to it. (<http://www.meop.net>).

## 582 **References**

- 583 Amblas, D., & Dowdeswell, J. A. (2018). Physiographic influences on dense shelf-water cas-  
 584 cading down the Antarctic continental slope. *Earth-Science Reviews*, 185(August),  
 585 887–900. Retrieved from <https://doi.org/10.1016/j.earscirev.2018.07.014>  
 586 doi: 10.1016/j.earscirev.2018.07.014
- 587 Baines, P. G., & Condie, S. (1998). Observations and Modelling of Antarctic Downslope  
 588 Flows: A Review. *OCEAN, ICE, AND ATMOSPHERE: INTERACTIONS AT THE*  
 589 *ANTARCTIC CONTINENTAL MARGIN. ANTARCTIC RESEARCH SERIES*, 75,  
 590 29–49. doi: 10.1029/ar075p0029
- 591 Cavalieri, D. J., & Martin, S. (1994). The contribution of Alaskan, Siberian, and Canadian  
 592 coastal polynyas to the cold halocline layer of the Arctic Ocean. *Journal of Geophysical*  
 593 *Research*, 99(C9). doi: 10.1029/94jc01169
- 594 de Boyer Montégut, C., Madec, G., Fischer, A. S., Lazar, A., & Iudicone, D. (2004).  
 595 Mixed layer depth over the global ocean: An examination of profile data and a profile-  
 596 based climatology. *Journal of Geophysical Research C: Oceans*, 109(12), 1–20. doi:  
 597 10.1029/2004JC002378
- 598 de Boer, A. M., Sigman, D. M., Toggweiler, J. R., & Russell, J. L. (2007). Effect of global  
 599 ocean temperature change on deep ocean ventilation. *Paleoceanography*, 22(2), 1–15.  
 600 doi: 10.1029/2005PA001242
- 601 Foster, T. D., & Carmack, E. C. (1976). Frontal zone mixing and Antarctic Bottom  
 602 water formation in the southern Weddell Sea. *Deep-Sea Research and Oceanographic*  
 603 *Abstracts*, 23(4), 301–317. doi: 10.1016/0011-7471(76)90872-X
- 604 Fox-Kemper, B., Hewitt, H. T., Xiao, C., Adalgeirsdottir, G., Drijfhout, S. S., Edwards,  
 605 T. L., . . . Yu, Y. (2021). Ocean, Cryosphere and Sea Level Change. *Climate Change*  
 606 *2021: The Physical Science Basis. Contribution of Working Group I to the Sixth*  
 607 *Assessment Report of the Intergovernmental Panel on Climate Change Science Basis.*  
 608 *Contribution of Working Group I to the Sixth Assessment Report of the Intergover,*  
 609 *2018(August), 1–257.*
- 610 Gordon, A. L., & Tchernia, P. L. (1972). Waters of the continental margin off Adélie Coast,

- 611 Antarctica. *Antarctic Research Series. Antarctica Oceanology II: The Australian—New*  
 612 *Zealand Sector, 19*, 59–69. doi: 10.1029/ar019p0059
- 613 Gordon, A. L., Zambianchi, E., Orsi, A., Visbeck, M., Giulivi, C. F., Whitworth, T., &  
 614 Spezie, G. (2004). Energetic plumes over the western Ross Sea continental slope.  
 615 *Geophysical Research Letters, 31*(21), 5–8. doi: 10.1029/2004GL020785
- 616 Herraiz-Borreguero, L., Church, J. A., Allison, I., Peña-Molino, B., Coleman, R., Tomczak,  
 617 M., & Craven, M. (2016). Basal melt, seasonal water mass transformation, ocean  
 618 current variability, and deep convection processes along the Amery Ice Shelf calving  
 619 front, East Antarctica. *Journal of Geophysical Research: Oceans, 121*(7), 4946–4965.  
 620 doi: 10.1002/2016JC011858
- 621 Herraiz-Borreguero, L., Coleman, R., Allison, I., Rintoul, S. R., Craven, M., & Williams,  
 622 G. D. (2015). Circulation of modified Circumpolar Deep Water and basal melt beneath  
 623 the Amery Ice Shelf, East Antarctica. *Journal of Geophysical Research: Oceans,*  
 624 *120*(4), 3098–3112. doi: 10.1002/2015JC010697
- 625 Jacobs, S. S. (2004). Bottom water production and its links with the thermohaline circula-  
 626 tion. *Antarctic Science, 16*(4), 427–437. doi: 10.1017/S095410200400224X
- 627 Jacobs, S. S., Helmer, H. H., Doake, C. S., Jenkins, A., & Frolich, R. M. (1992). Melting  
 628 of ice shelves and the mass balance of Antarctica. *Journal of Glaciology, 38*(130),  
 629 375–387. doi: 10.1017/S0022143000002252
- 630 Kitade, Y., Shimada, K., Tamuta, T., Williams, G., Aoki, S., Fukamachi, Y., . . . Ohshima,  
 631 K. (2014). Antarctic Bottom Water production from the Vincennes Bay Polynya, East  
 632 Antarctica. *Geophysical Research Letters, 41*, 9–13. doi: doi:10.1002/2014GL059971.
- 633 Kobayashi, T. (2018). Rapid volume reduction in Antarctic Bottom Water off the  
 634 Adélie/George V Land coast observed by deep floats. *Deep-Sea Research Part I:*  
 635 *Oceanographic Research Papers, 140*, 95–117. Retrieved from [https://doi.org/](https://doi.org/10.1016/j.dsr.2018.07.014)  
 636 [10.1016/j.dsr.2018.07.014](https://doi.org/10.1016/j.dsr.2018.07.014) doi: 10.1016/j.dsr.2018.07.014
- 637 Labrousse, S., Williams, G., Tamura, T., Bestley, S., Sallée, J. B., Fraser, A. D., . . .  
 638 Charrassin, J. B. (2018). Coastal polynyas: Winter oases for subadult southern  
 639 elephant seals in East Antarctica. *Scientific Reports, 8*(1), 1–15. doi: 10.1038/  
 640 s41598-018-21388-9
- 641 Liu, C., Wang, Z., Cheng, C., Wu, Y., Xia, R., Li, B., & Li, X. (2018). On the Modified  
 642 Circumpolar Deep Water Upwelling Over the Four Ladies Bank in Prydz Bay, East  
 643 Antarctica. *Journal of Geophysical Research: Oceans, 123*(11), 7819–7838. doi: 10  
 644 .1029/2018JC014026
- 645 Malpress, V., Bestley, S., Corney, S., Welsford, D., Labrousse, S., Sumner, M., & Hindell, M.  
 646 (2017). Bio-physical characterisation of polynyas as a key foraging habitat for juvenile  
 647 male southern elephant seals (*Mirounga leonina*) in Prydz Bay, East Antarctica. *PLoS*  
 648 *ONE, 12*(9), 1–24. doi: 10.1371/journal.pone.0184536
- 649 Massom, R. A., Harris, P. T., Michael, K. J., & Potter, M. J. (1998). The distribution and  
 650 formative processes of latent-heat polynyas in East Antarctica. *Annals of Glaciology,*  
 651 *27*, 420–426. doi: 10.3189/1998aog27-1-420-426
- 652 McMahan, C. R., Roquet, F., Baudel, S., Belbeoch, M., Bestley, S., Blight, C., . . . Wood-  
 653 ward, B. (2021). Animal Borne Ocean Sensors – AniBOS – An Essential Component  
 654 of the Global Ocean Observing System. *Frontiers in Marine Science, 8*(November),  
 655 1–21. doi: 10.3389/fmars.2021.751840
- 656 Narayanan, A., Gille, S. T., Mazloff, M. R., & Murali, K. (2019). Water Mass Char-  
 657 acteristics of the Antarctic Margins and the Production and Seasonality of Dense  
 658 Shelf Water. *Journal of Geophysical Research: Oceans, 124*(12), 9277–9294. doi:  
 659 10.1029/2018JC014907
- 660 Nihashi, S., & Ohshima, K. I. (2015). Circumpolar mapping of antarctic coastal polynyas  
 661 and landfast sea ice: Relationship and variability. *Journal of Climate, 28*(9), 3650–  
 662 3670. doi: 10.1175/JCLI-D-14-00369.1
- 663 Ohshima, K. I., Fukamachi, Y., Williams, G. D., Nihashi, S., Roquet, F., Kitade, Y.,  
 664 . . . Wakatsuchi, M. (2013). Antarctic Bottom Water production by intense sea-ice  
 665 formation in the Cape Darnley polynya. *Nature Geoscience, 6*(3), 235–240. Retrieved

- 666 from <http://dx.doi.org/10.1038/ngeo1738> doi: 10.1038/ngeo1738
- 667 Orsi, A. H., Johnson, G. C., & Bullister, J. L. (1999). Circulation, mixing, and production  
668 of Antarctic Bottom Water. *Progress in Oceanography*, *43*(1), 55–109. doi: 10.1016/  
669 S0079-6611(99)00004-X
- 670 Orsi, A. H., Smethie, W. M., & Bullister, J. L. (2002). On the total input of Antarctic waters  
671 to the deep ocean: A preliminary estimate from chlorofluorocarbon measurements.  
672 *Journal of Geophysical Research: Oceans*, *107*(8). doi: 10.1029/2001jc000976
- 673 Orsi, A. H., & Wiederwohl, C. L. (2009). A recount of Ross Sea waters. *Deep-Sea Research*  
674 *Part II: Topical Studies in Oceanography*, *56*(13-14), 778–795. Retrieved from [http://](http://dx.doi.org/10.1016/j.dsr2.2008.10.033)  
675 [dx.doi.org/10.1016/j.dsr2.2008.10.033](http://dx.doi.org/10.1016/j.dsr2.2008.10.033) doi: 10.1016/j.dsr2.2008.10.033
- 676 Portela, E., Rintoul, S. R., Bestley, S., Herraiz-Borreguero, L., van Wijk, E., McMahon,  
677 C. R., ... Hindell, M. (2021). Seasonal transformation and spatial variability of  
678 water masses within MacKenzie polynya, Prydz Bay. *Journal of Geophysical Research:*  
679 *Oceans*, *126*, 1–21. doi: 10.1029/2021jc017748
- 680 Purkey, S. G., & Johnson, G. C. (2012). Global contraction of Antarctic Bottom Water  
681 between the 1980s and 2000s. *Journal of Climate*, *25*(17), 5830–5844. doi: 10.1175/  
682 JCLI-D-11-00612.1
- 683 Ribeiro, N., Herraiz-Borreguero, L., Rintoul, S. R., McMahon, C. R., Hindell, M., Harcourt,  
684 R., & Williams, G. (2021). Warm Modified Circumpolar Deep Water Intrusions  
685 Drive Ice Shelf Melt and Inhibit Dense Shelf Water Formation in Vincennes Bay, East  
686 Antarctica. *Journal of Geophysical Research: Oceans*, *126*(8), 1–17. doi: 10.1029/  
687 2020jc016998
- 688 Rintoul, S. R. (1998). On the Origin and Influence of Adélie Land Bottom Water.  
689 *ANTARCTIC RESEARCH SERIES. OCEAN, ICE, AND ATMOSPHERE: INTER-*  
690 *ACTIONS AT THE ANTARCTIC CONTINENTAL MARGIN*, *75*, 151–171. doi:  
691 10.1029/ar075p0151
- 692 Roquet, F., Williams, G., Hindell, M. A., Harcourt, R., McMahon, C., Guinet, C., ... Fedak,  
693 M. (2014). A Southern Indian Ocean database of hydrographic profiles obtained with  
694 instrumented elephant seals. *Scientific Data*, *1*, 1–10. doi: 10.1038/sdata.2014.28
- 695 Schaffer, J., Timmermann, R., Arndt, J. E., Rosier, S. H. R., Anker, P. G. D., Callard,  
696 S. L., ... Roberts, D. H. (2019). *An update to Greenland and Antarctic ice*  
697 *sheet topography, cavity geometry, and global bathymetry (RTopo-2.0.4)* [data set].  
698 PANGAEA. Retrieved from <https://doi.org/10.1594/PANGAEA.905295> doi:  
699 10.1594/PANGAEA.905295
- 700 Shapiro, G. I., Huthnance, J. M., & Ivanov, V. V. (2003). Dense water cascading off  
701 the continental shelf. *Journal of Geophysical Research: Oceans*, *108*(12), 1–19. doi:  
702 10.1029/2002jc001610
- 703 Silvano, A., Rintoul, S. R., & Herraiz-Borreguero, L. (2016). Ocean-ice shelf interaction in  
704 East Antarctica. *Oceanography*, *29*(4), 130–143. doi: 10.5670/oceanog.2016.105
- 705 Silvano, A., Rintoul, S. R., Peña-Molino, B., Hobbs, W. R., Van Wijk, E., Aoki, S., ...  
706 Williams, G. D. (2018). Freshening by glacial meltwater enhances melting of ice  
707 shelves and reduces formation of Antarctic Bottom Water. *Science Advances*, *4*(4),  
708 1–12. doi: 10.1126/sciadv.aap9467
- 709 Smith, J. A., Hillenbrand, C.-D., Pudsey, C. J., Allen, C. S., & Graham, A. G. (2010).  
710 The presence of polynyas in the Weddell Sea during the Last Glacial Period with  
711 implications for the reconstruction of sea-ice limits and ice sheet history. *Earth and*  
712 *Planetary Science Letters*, *296*, 287–298. doi: <https://doi.org/10.1016/j.epsl.2010.05>  
713 .008
- 714 Tamura, T., Ohshima, K. I., Fraser, A. D., & Williams, G. D. (2016). Sea ice production  
715 variability in Antarctic coastal polynyas. *Journal of Geophysical Research: Oceans*,  
716 1–14. doi: 10.1002/2015JC011537. Received
- 717 Tamura, T., Ohshima, K. I., Markus, T., Cavalieri, D. J., Nishashi, S., & Hirasawa, N.  
718 (2007). Estimation of thin ice thickness and detection of fast ice from SSM/I data  
719 in the Antarctic Ocean. *Journal of Atmospheric and Oceanic Technology*, *24*(10),  
720 1757–1772. doi: 10.1175/JTECH2113.1

- 721 Van Wijk, E., & Rintoul, S. R. (2014). Geophysical Research Letters. *Geophysical Research*  
722 *Letters*(April), 6298–6305. doi: doi:10.1002/2013GL058921
- 723 Williams, G. D., Bindoff, N. L., Marsland, S. J., & Rintoul, S. R. (2008). Formation and  
724 export of dense shelf water from the Adélie depression, East Antarctica. *Journal of*  
725 *Geophysical Research: Oceans*, 113(4), 1–12. doi: 10.1029/2007JC004346
- 726 Williams, G. D., Herraiz-Borreguero, L., Roquet, F., Tamura, T., Ohshima, K. I., Fuka-  
727 machi, Y., ... Hindell, M. (2016). The suppression of Antarctic bottom water  
728 formation by melting ice shelves in Prydz Bay. *Nature Communications*, 7(6),  
729 1–9. Retrieved from <http://dx.doi.org/10.1038/ncomms12577> doi: 10.1038/  
730 ncomms12577
- 731 Xu, Z., Gao, G., Xu, J., & Shi, M. (2017). The evolution of water property in the Mackenzie  
732 Bay polynya during Antarctic winter. *Journal of Ocean University of China*, 16(5),  
733 766–774. doi: 10.1007/s11802-017-3286-8